Journal of Computational Applied Mechanics 2022, 53 (3): 414-430

DOI: 10.22059/jcamech.2022.347011.745

RESEARCH PAPER

Numerical study of Casson nanofluid over an elongated surface in presence of Joule heating and viscous dissipation: Buongiorno model analysis

Kharabela Swain [a,*], Manoranjan Mishra [a], Abha Kumari [b]

[a] *Department of Mathematics, Gandhi Institute for Technology, Bhubanewar-752054, India*
[b] *Department of Mathematics, Nirmala College, Ranchi, Jharkhand-834002, India*

Abstract

Nanoparticles (NPs) have wide engineering and industrial applications including improving heat transfer, cooling and heating processes, refrigeration, and medical sciences like cancer treatment etc. Further, Buongiorno model is used to determine how Brownian motion and thermophoresis affect the unsteady 2D flow of Casson nanofluid (NF) over a stretching sheet entrenched in a porous medium. The flow is exposed to an exponential heat source, thermal radiation, dissipation, Joule heating, and transverse magnetic field. The diffusion of chemically reactive NPs to base fluid has been considered. The leading equations of flow model admit similarity solution and reduce to non-linear ODEs by appropriate similarity renovations and elucidated numerically by MATLAB software using bvp4c code. It is found that incidence of NPs in the base fluid reduces the shearing stress at the plate surface so as to avoid back flow. Thermophoresis favours the rise in volume fraction and temperature of the nanofluid. Use of high-Prandtl number base fluid and NP of high thermal conductivity could be of practical use to increase the rate of heat transfer and to avoid NP accumulation.

Keywords: Stretching sheet; Casson fluid; thermophoresis; Brownian motion; thermal radiation.

1. Introduction

Flow of an incompressible viscous fluid over an elongating sheet has significant manufacturing and industrial uses such as drawing glass fibres, producing crystals, extruding plastic, making paper, etc. Crane [1] established a closed form similarity solution to a flow due to stretching sheet. Mahapatra and Gupta [2] studied the stagnation point flow towards an extending sheet. In recent years, study of non-Newtonian fluid has gained more importance due to its industrial applications. Further, Misra and Sinha [3] studied the biological applications of flow on stretching surface.

Casson fluid is a form of non-Newtonian fluid due to its rheological properties in regard to the shear stress-strain connection. Above a critical stress value, it behaves like a Newtonian fluid, but at low shear and strain, it behaves like an elastic solid. Authors like Mukhopadhyay et al. [4], Seth et al. [5], Gopal et al. [6], and Sreenivasulu et al. [7] explored their study on Casson fluid past an extending sheet by taking various fluid properties. El-Aziz and Afify [8] studied the Casson fluid flow over a stretching sheet with entropy generation. Das et al. [9] considered the mass and heat transfer analysis on unsteady flow Casson fluid past a flat plate. Further, several authors [10-17] have studied the Casson NF flow by taking different flow models. Recently, Mahanthesh et al. [18] inspected the effect of

* Corresponding author. Tel.: +91 6742561445.
E-mail address: kharabela1983@gmail.com

exponential heat source on NF flow over a stretched disk.

Asemi et al. [19] studied nanoscale mass detection based on vibrating piezoelectric ultrathin films. Asemi et al. [20, 21] studied the vibration of double-piezoelectric-nanoplate systems based on nonlocal elasticity theory. Baghani et al. [22] studied the stability analysis of the rotating nanobeam in a nonuniform magnetic field. Danesh et al. [23] analysed the tapered nanorod based on nonlocal elasticity theory and differential quadrature method. Farajpour et al. [24-30] studied the buckling analysis of variable thickness considering different geometry. Farajpour et al. [31] studied the vibration of piezoelectric nanofilm-based electromechanical sensors through higher-order non-local strain gradient theory. Ghayour et al. [32] examined the wave propagation approach to fluid filled submerged visco-elastic finite cylindrical shells. Goodarzi et al. [33] investigated the effect of pre-stressed on vibration frequency of rectangular nanoplate. Mohammadi et al. [19-53], Moosavi et al. [35] and Safarabadi et al. [46] studied the vibration analysis of graphene sheet considering various conditions.

Prasad et al. [54] studied slip flow of chemically reacting Casson fluid over a porous slender sheet. Raju et al. [55] examined the impact of induced magnetic field on stagnation flow of a Casson fluid. Amanulla et al. [56-59] studied the non-Newtonian fluid flow under different conditions. Upadhya et al. [60] and Babu et al. [61] studied the free convective flow of nanofluids. Nagendra et al. [62, 63] studied the flow of non-Newtonian fluid with slip boundary conditions. Authors such as Kumar at al. [64], Hobiny et al. [65], and Horrigue et al. [66] studied the fractional-order thermoelastic wave assessment. Many authors [67-69] have numerically studied the fractional time derivative. Hayat et al. [70] studied the flow of nanofluid with convective boundary conditions. Ram et al. [71] studied the effect of heat source/sink on the variable reactive Casson fluid through an infinite plate. Shamshuddin et al. [72-74] studied the nanofluid flow considering different flow models. Mabood et al. [75] studied the thermophoresis and Brownian motion on micropolar fluid flow towards continuously moving flat plate. Rajput et al. [76] studied the non-Newtonian radiative Casson fluid flow over a vertical plate.

In view of the above cited literature survey, the objective of the present analysis is laid down as follows. The momentum transport equation of Casson nanofluid has been modified due to temperature as well as space dependent free stream (potential flow) stretching. Further, the presence of two body forces, one of electro-magnetic force and another evolved due to permeability of the saturated porous medium embedding the stretching sheet through which flow occurs. Most importantly, the heat equation becomes more complex due to inclusion of the followings: inclusion of Brownian motion represented by Brownian diffusion coefficient, thermophoresis, thermal radiation, Joulian and viscous dissipation. In addition to those complex thermal and molecular processes, the presence of time, space and temperature dependent exponential heat sink/source has made the analysis unique, hardly studied earlier. Further, the current analysis brings to its fold the viscous flow by letting $\gamma \to \infty$ and constant surface condition by letting the coefficients $T_0, C_0 \to 0$.

2. Design of the problem

Consider an unsteady, laminar 2D flow of a Casson NF over an elongated sheet in presence of porous matrix as shown in Fig. 1. The *y*-axis is taken normal to the plate and the flow confined to the plane $y > 0$, is due to elongated bounding surface and free stream. A transverse magnetic field of strength B_0 is applied along *y*-axis. The interaction of the conducting fluid with transversely applied magnetic field generates an electromagnetic force which resists the fluid motion. We have restricted our discussion to low magnetic Reynolds number to avoid the effect of induced magnetic field that paves the way for future study. The constitutive equation for an isotropic and incompressible flow of Casson fluid is given by [77]

$$\tau_{ij} = \begin{cases} 2\left(\mu_B + \dfrac{p_y}{\sqrt{2\pi}}\right)e_{ij}, \pi > \pi_c \\ 2\left(\mu_B + \dfrac{p_y}{\sqrt{2\pi_c}}\right)e_{ij}, \pi < \pi_c \end{cases}$$

where μ_B, p_y are the plastic dynamic viscosity, yield stress of the fluid respectively, $\pi = e_{ij}e_{ij}$, e_{ij} is the $(i, j)^{th}$ component of the deformation rate and π_c is the critical value of π, based on non-Newtonian model.

The leading equations with prescribed boundary conditions of the unsteady incompressible Casson nanofluid flow following [15] are:

$$0 = u_x + v_y, \tag{1}$$

$$(U_e)_t + U_e (U_e)_x + \upsilon_f \left(1+\gamma^{-1}\right) u_{yy} - \sigma B_0^2 \rho_f^{-1} (u - U_e) - \upsilon_f K_p^{*-1} (u - U_e) = u_t + u u_x + v u_y, \tag{2}$$

$$\begin{aligned} &\alpha_f T_{yy} + \tau \left[D_B T_y C_y + \frac{D_T}{T_\infty} T_y^{\,2} \right] - \frac{1}{(\rho c)_f} (q_r)_y + \frac{\sigma B_0^2}{(\rho c)_f} u^2 \\ &+ \frac{\mu_f}{(\rho c)_f} \left(1+\gamma^{-1}\right) u_y^{\,2} + \frac{Q}{(\rho c)_f} (T_w - T_\infty) e^{-\sqrt{\frac{a}{\upsilon_f (1-\lambda t)}} y} = T_t + u T_x + v T_y, \end{aligned} \tag{3}$$

$$D_B C_{yy} + \frac{D_T}{T_\infty} T_{yy} = C_t + u C_x + v C_y, \tag{4}$$

$$\left. \begin{aligned} &u = u_w(x,t) = ax(1-\lambda t)^{-1}, v = 0, T = T_w(x,t), C = C_w(x,t), \\ &u = U_e(x,t) = bx(1-\lambda t)^{-1}, T \to T_\infty, C \to C_\infty. \end{aligned} \right\} \tag{5}$$

Using Rosseland approximation [20]

$$q_r = -\frac{4\sigma^*}{3k^*} \left(T^4\right)_y \Rightarrow (q_r)_y = -\frac{16\sigma^* T_\infty^3}{3k^*} T_{yy},$$

where σ^* and k^* are respectively known as Stefan-Boltzmann constant and absorption coefficient.

The value of $(q_r)_y$ is substituted in equation (3) for further analysis in reducing non-dimensional form.

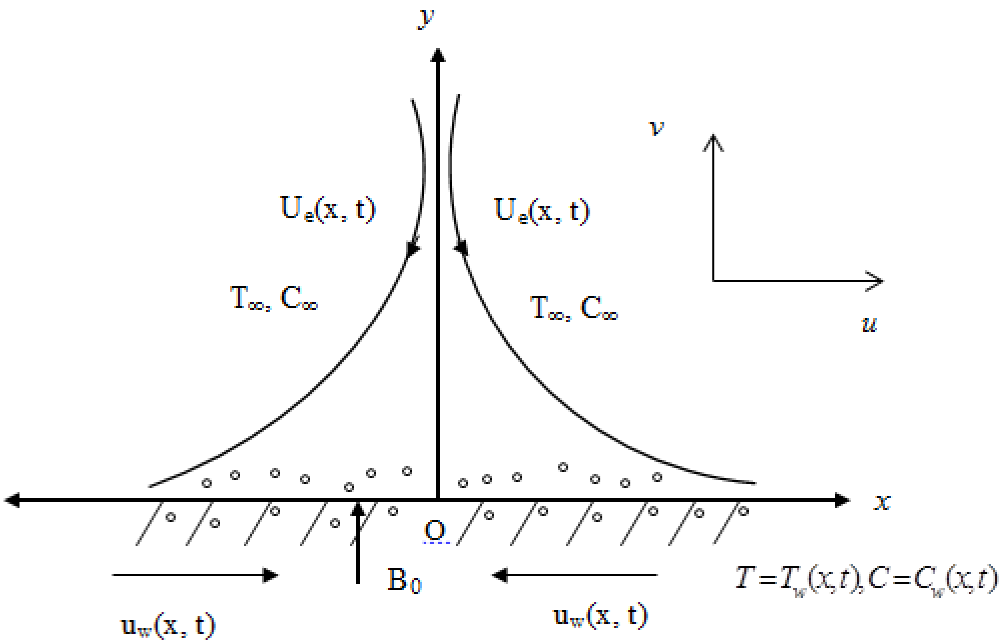

Fig 1: Flow geometry

The ensuing similarity variables and transformations have been entreated.

$$u = \frac{\partial \psi}{\partial y}, v = -\frac{\partial \psi}{\partial x}, \; \eta = \sqrt{\frac{a}{\upsilon_f (1-\lambda t)}} y, \psi = \sqrt{\frac{a \upsilon_f}{(1-\lambda t)}} x f(\eta),$$

$$T = T_\infty + T_0\left[\frac{ax^2}{(1-\lambda t)^2}\right]\theta(\eta), C = C_\infty + C_0\left[\frac{ax^2}{(1-\lambda t)^2}\right]\phi(\eta).$$

Now, the equations (1) - (5) convert

$$f''' = -\left(1+\gamma^{-1}\right)^{-1}\left[ff'' - f'^2 - \left(M+K_p\right)\left(f'-\beta\right) + \beta^2 - S\left(\frac{1}{2}\eta f'' + f' - \beta\right)\right], \quad (6)$$

$$\theta'' = \Pr\left(1+\frac{4}{3}R\right)^{-1}\begin{bmatrix} S\left(\frac{1}{2}\eta\theta' + 2\theta\right) - f\theta' + 2f'\theta - Nb\theta'\phi' - Nt\theta'^2 \\ -MEcf'^2 - Ec\left(1+\gamma^{-1}\right)f''^2 - Q_e\exp\left(-n\eta\right)\end{bmatrix}, \quad (7)$$

$$\phi'' = Sc\left[S\left(\frac{1}{2}\eta\phi' + 2\phi\right) - f\phi' + 2f'\phi - \frac{Nt}{ScNb}\theta''\right], \quad (8)$$

$$\left.\begin{array}{l} f'(0)=1, f(\eta)=0, \theta(\eta)=1, \phi(\eta)=1, \\ f'(\infty)=\beta, \theta(\infty)=0, \phi(\infty)=0. \end{array}\right\} \quad (9)$$

Physical quantities of engineering interest:

Skin friction coefficient $C_f = \frac{\mu}{\rho_f U_w^2}\left(\frac{\partial u}{\partial y}\right)_{y=0} \Rightarrow \mathrm{Re}_x^{0.5} C_{fx} = f''(0),$

local Nusselt number $Nu_x = \frac{-x}{(T_w - T_\infty)}\left[\frac{\partial T}{\partial y} - \frac{4\sigma^*}{3k'^*}\left(\frac{\partial T^4}{\partial y}\right)\right]_{y=0} \Rightarrow \mathrm{Re}_x^{-0.5} Nu_x = -\left(1+\frac{4}{3}R\right)\theta'(0),$ and local

Sherwood number $Sh_x = \frac{-x}{(C_w - C_\infty)}\left(C_y\right)_{y=0} \Rightarrow \mathrm{Re}_x^{-0.5} Sh_x = -\phi'(0).$

The steady-state flow can be retrieved by taking $S = 0$.

3. Results and discussion

The set of non-linear ODEs (6) - (9) are solved numerically by MATLAB software using bvp4c code. The pressure gradient has been evaluated by the potential flow. No cross flow exists at the surface. The wall temperature and concentration are more than free stream temperature and concentration since $1-\lambda t > 0$ and $a > 0$. Thus, there is a thermal energy as well as mass transfer occur from the bounding surface to the flow domain. In view of similarity variable and transformations, the study of squeezing flow as well as low surface temperature and concentration are constrained so that only stretching is possible in the present study. Due to stretching ratio parameter β $\left(\beta < 1\right)$, the inverted boundary layer is formed and hence the effects of parameters are reversed. Therefore, the presentation and discussion thereof are tacitly dealt with. The validity of the results is verified with the work conveyed in the literature and revealed in Table 1. Further, throughout the computation, we fixed the values of the non-dimensional parameters as $M = K_p = \gamma = \beta = 0.5, S = 0.3, Nb = Nt = R = Ec = Q_e = 0.1,$ $\Pr = 5, n = 2,$ and $Sc = 1$ except those the particular variation is deployed in the corresponding figure.

Table 1: Computation of $f''(0)$ when $M = Kp = S = 0, \gamma \to \infty.$

β	Das et al. [15]	Swain et al. [78]	Rout and Mishra [17]	Present study
0.1	-0.969328	-0.96965625	-0.96966	-0.9696514
0.2	-0.918098	-0.91816450	-0.91816	-0.9181601
0.5	-0.667301	-0.66726432	-0.66726	-0.6672609

2	2.017467	2.01750252	2.017502	2.0175025
3	4.729406	4.72928082	---	4.7292808

The unsteadiness of the flow reduces the momentum transport but enhances the thermal energy irrespective of the impacts of other parameters. Figs. 2 - 4 show the effects of M, β, γ K_p on velocity distribution. The boundary layer is formed when $\beta > 1$ i.e. with higher rate of free stream stretching than bounding surface. The inverted boundary layer is formed for $\beta < 1$. The magnetic (M) and porosity (K_p) parameters reduce the velocity due to resistive Lorentz force and existence of porous matrix respectively and the effect is reversed in case of inverted boundary layer. The effect of γ is to reduce the velocity, resulting a thinning of boundary layer.

Figs. 5-9 depict the temperature distribution for various values of the parameters. It is seen that an increase in Ec and R increases the temperature as increase in Ec and R contribute to higher thermal energy (Figs. 5 and 6). Physically, Ec represents the amount of heat energy that is added as a result of viscous dissipation. Additionally, it can be observed that temperature rises as heat source parameter values rise, and in the presence of sink; it decreases (Fig. 7). Fig. 8 shows that temperature decreases with higher exponential index (n) which is also evident from equation (4) as the exponent is negative but higher stretching rate decreases the temperature since it quickens the process of diffusion of thermal energy. Fig. 9 shows the distribution of temperature as well as volume fraction of NP. It is evident that an increase in Brownian motion parameter (Nb), increases the thermal energy, and hence the temperature but the reverse effect is well marked in case of solutal concentration/volume fraction. In case of thermophoresis parameter (Nt), both volume fraction and temperature get accelerated with thermophoretic processes.

Figs. 10 and 11 depict the solutal concentration of NP. It is seen that higher stretching as well as higher Schmidt number (Sc) depletes the concentration level. Since both higher rate stretching and Schmidt number (heavier species) decelerates the mass diffusion contributing to thinner solutal boundary layer. From Fig. 11, it is evident that unsteady parameter decreases the concentration but Casson fluidity enhances it. It is oberved that slight instability is marked in concentration distribution for low Sc i.e., for lighter species and Casson parameter (γ).

Table 2 shows the variations of $-f''(0)$, $-\theta'(0)$ and $-\phi'(0)$ for different values of parameters. It is perceived that for fixed values of other parameters, the wall shear stress $\{-f''(0)\}$ enhances with the rise in the values of M and S, whereas it declines with increase in the value of β. In fact, Fig. 2 corroborates this observation as increase in M leads to decrease in velocity gradient at the surface for $\beta > 1$ as well as $\beta < 1$. Therefore, it is suggested that the magnetic intensity is to be reduced to decrease the shear at the bounding surface. Further, it is concluded that higher the unsteadiness, greater the shearing stress at the bounding surface. Moreover, the rates of heat transfer and solutal concentration rise with β and S but in case of M, rate of heat transfer declines but the rate of solutal concentration increases. It is perceived that $-\theta'(0)$ increases with increase in $\Pr$ as well as strength of exponential heat sink $(Q_e < 0)$ whereas $-\phi'(0)$ decreases. It is important to remark that Ec, Sc and exponential heat source $(Q_e > 0)$ affect $-\theta'(0)$ and $-\phi'(0)$ adversely as compared to that of $\Pr$ and $(Q_e < 0)$. This interesting result admits following physical interpretation. Lower Prandtl fluids possess greater thermal conductivity so that, diffusion of heat from the sheet is faster than higher Prandtl fluids. The above results are pertinent to the base liquids without the presence of NPs. However, according to Koo and Kleinstreuer [78], the inclusion of 20-nm copper NPs at modest volume fractions (1 to 4%) to high Prandtl number fluids considerably improves the heat transfer performance of a microchannel heat sink [79]. So use of high-Prandtl-number BFs and NPs of high thermal conductivity could be of practical use to increase the heat transfer and to avoid NP accumulation. The effect of increase in viscous dissipation parameter (Ec) is to reduce the wall temperature gradient $-\theta'(0)$ as an increase in Ec increases the temperature since more heat energy is stored up in the fluid due to frictional heating. Further, it is to note that higher Sc (heavier species of diffusion) and exponential heat source $(Q_e > 0)$ also reduce $-\phi'(0)$. But most interestingly, the rate of solutal concentration at the wall shows the opposite effect compared to rate of heat transfer. This may be attributed to the fact that higher thermal energy enhances the solutal diffusion causing the fall of concentration and hence, the flux at the wall. One more point is to note that in the present analysis, no significant effect of R, Ec and Sc on the force coefficient is marked. Thus, it is concluded that presence of NPs in the BF reduces the shearing effect at the plate surface so that it may impose stability or avoid back flow (flow separation) in the downstream.

4. Concluding remarks

The following key findings are as follows:

- The unsteadiness of the flow reduces the momentum transport but enhances the thermal energy irrespective of the effects of other parameters.
- The stretching ratio of free stream and plate surface plays a vital role in the formation of boundary layer and inverted boundary layer causing the flow reversal.
- Thermophoresis favours the rise in volume fraction and temperature of the nanofluid.
- Unsteadiness flow decreases the level of concentration but Casson fluidity enhances it.
- Use of high-Prandtl number BF and NP of high thermal conductivity could be of practical use to increase the rate of heat transfer and to avoid NP accumulation.
- The presence of NPs in the BF reduces the shearing stress at the plate surface so as to avoid back flow.

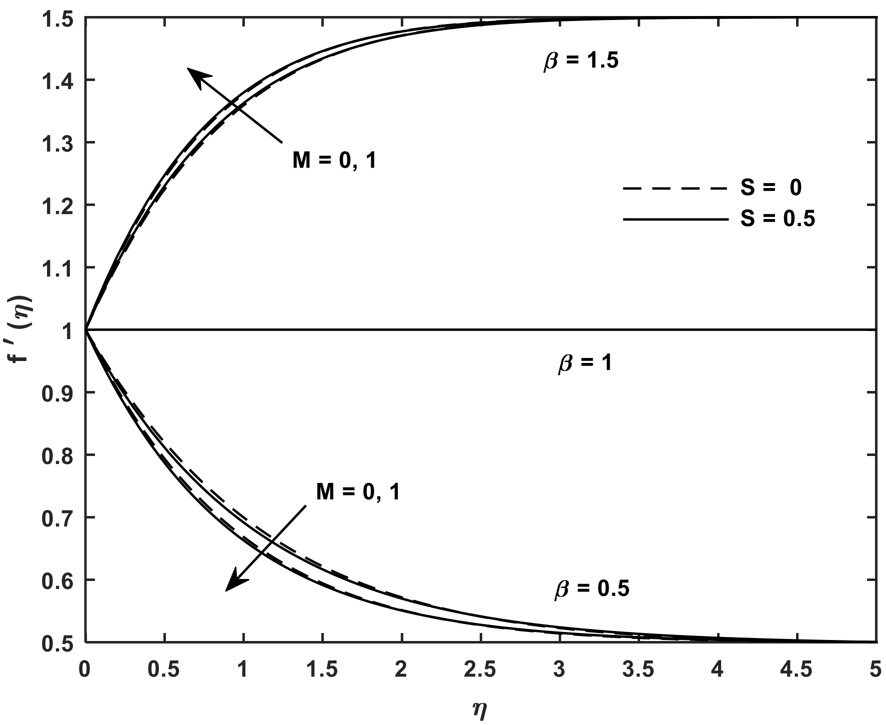

Fig 2: Velocity distributions versus M and β

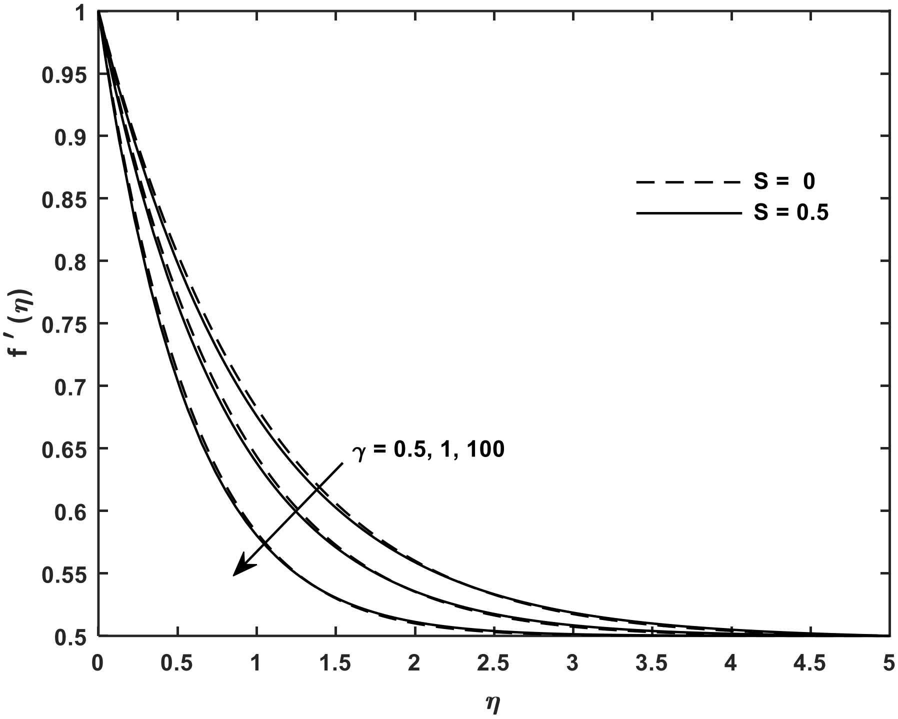

Fig 3: Velocity distributions versus γ

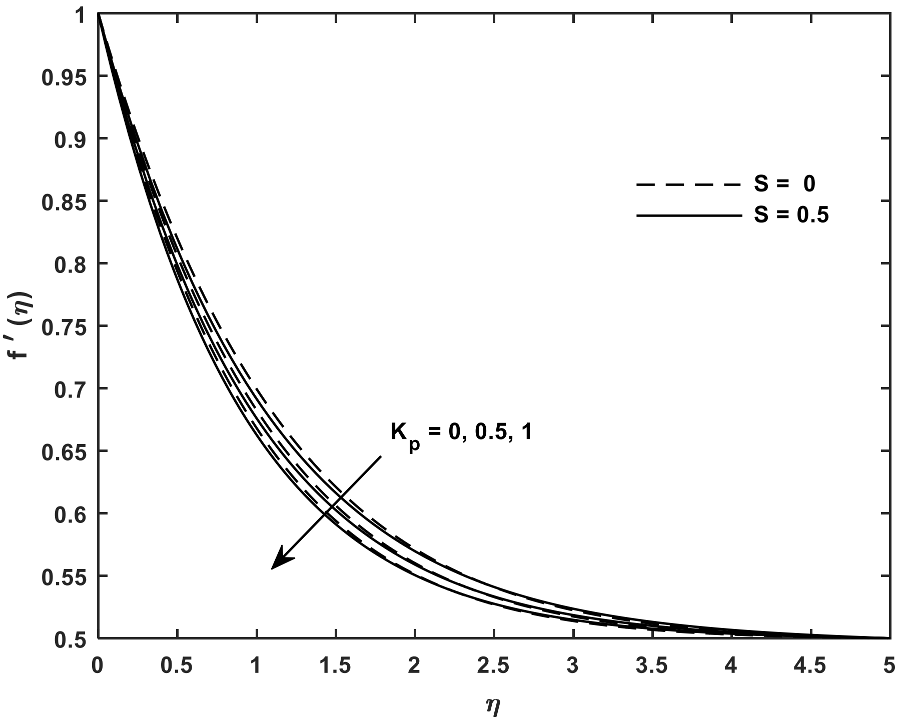

Fig 4: Velocity distributions versus K_p

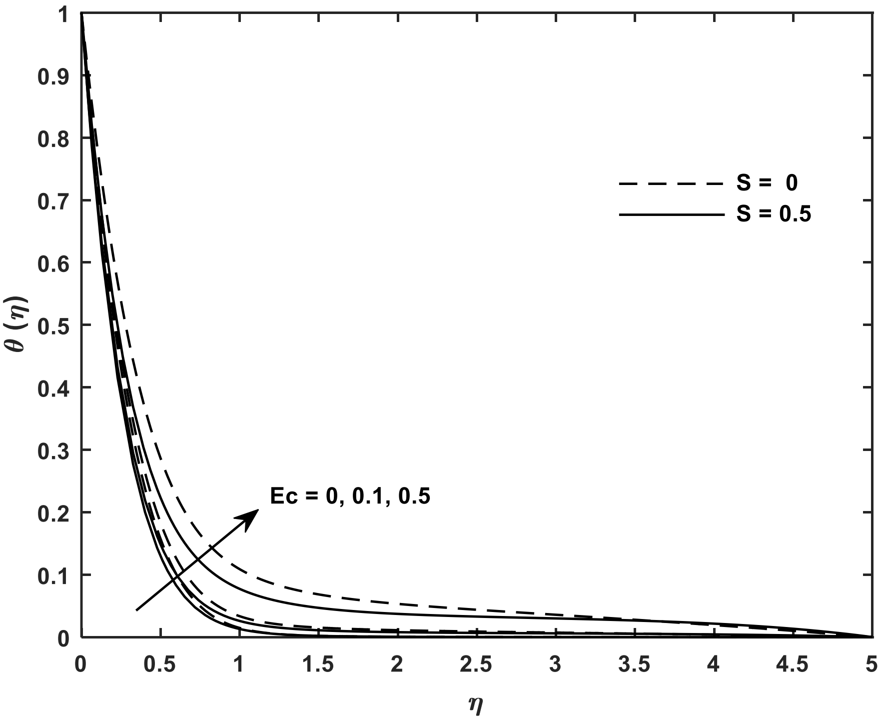

Fig 5: Temperature distributions versus Ec

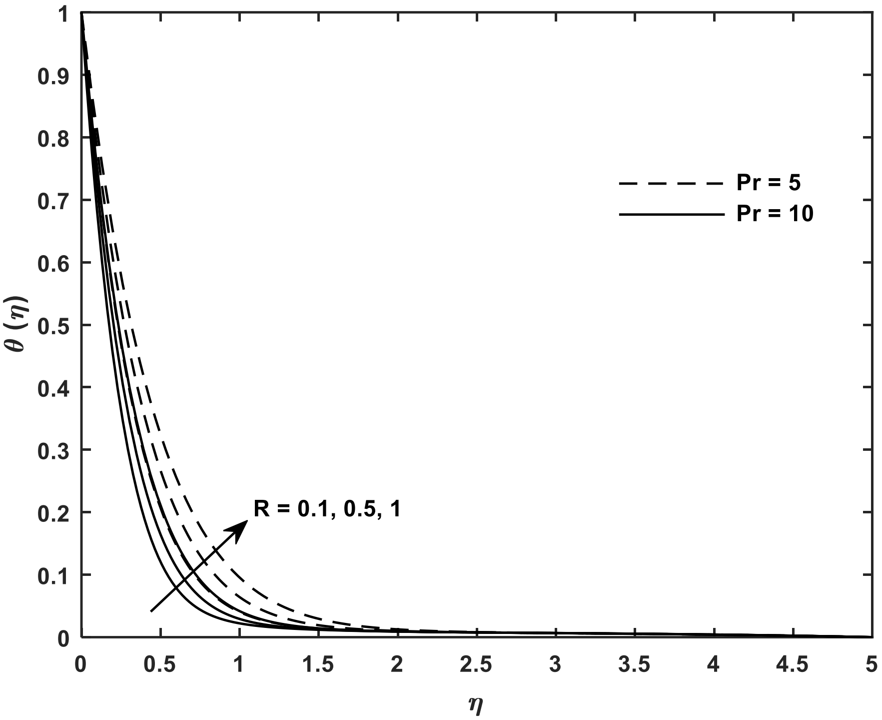

Fig 6: Temperature distributions versus R

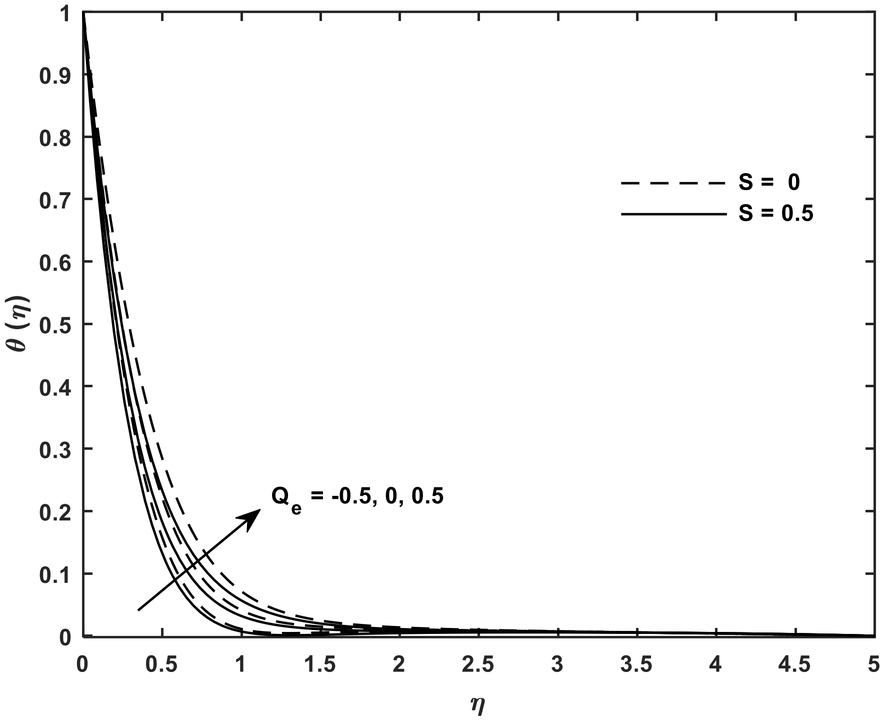

Fig 7: Temperature distributions versus Q_e

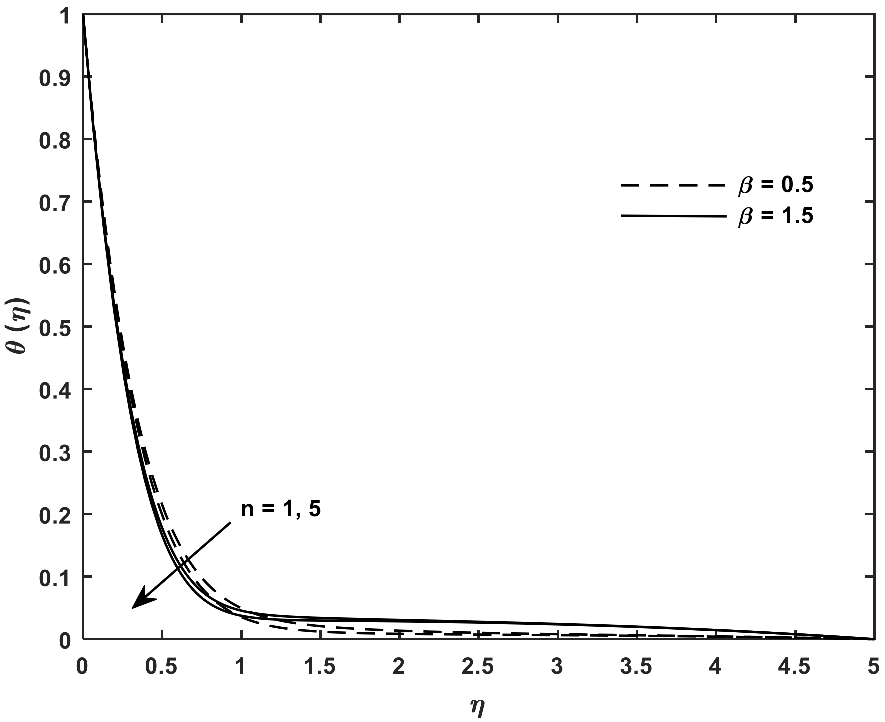

Fig 8: Temperature distributions versus n **and** β

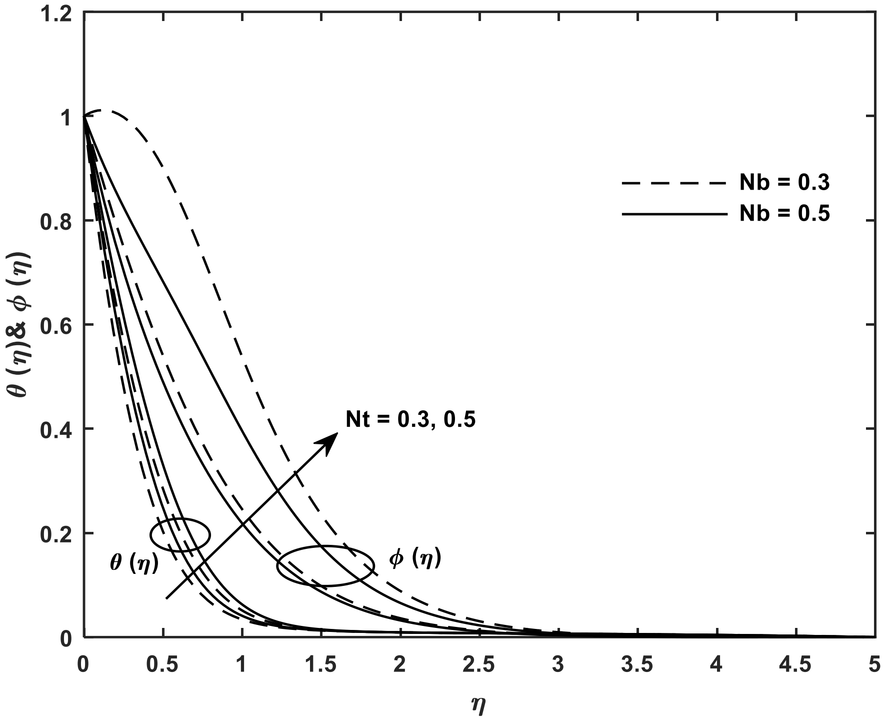

Fig 9: Temperature and concentration distributions versus Nb **and** Nt

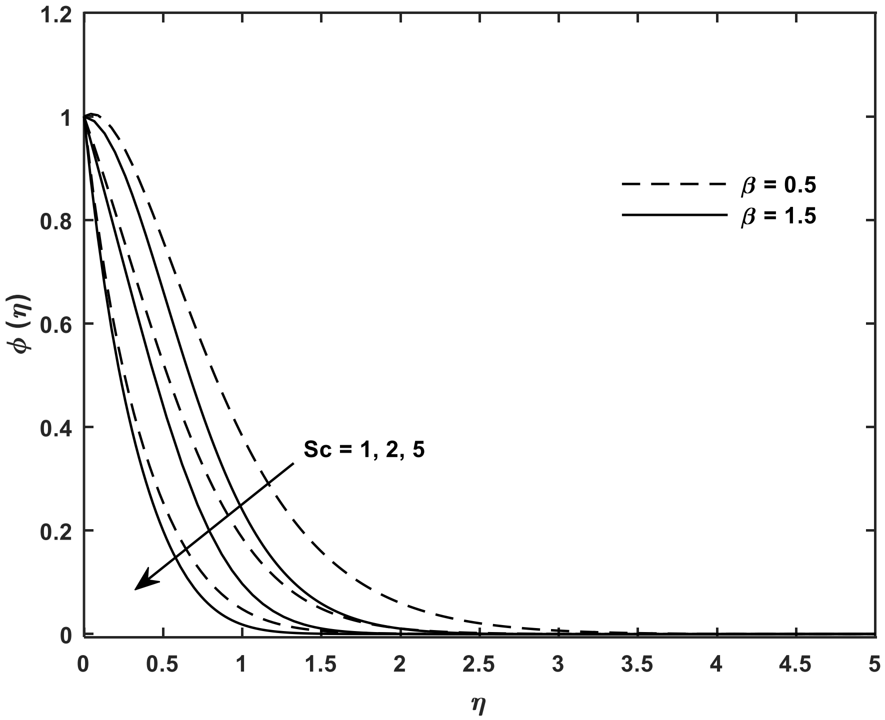

Fig 10: Concentration distributions versus Sc **and** β

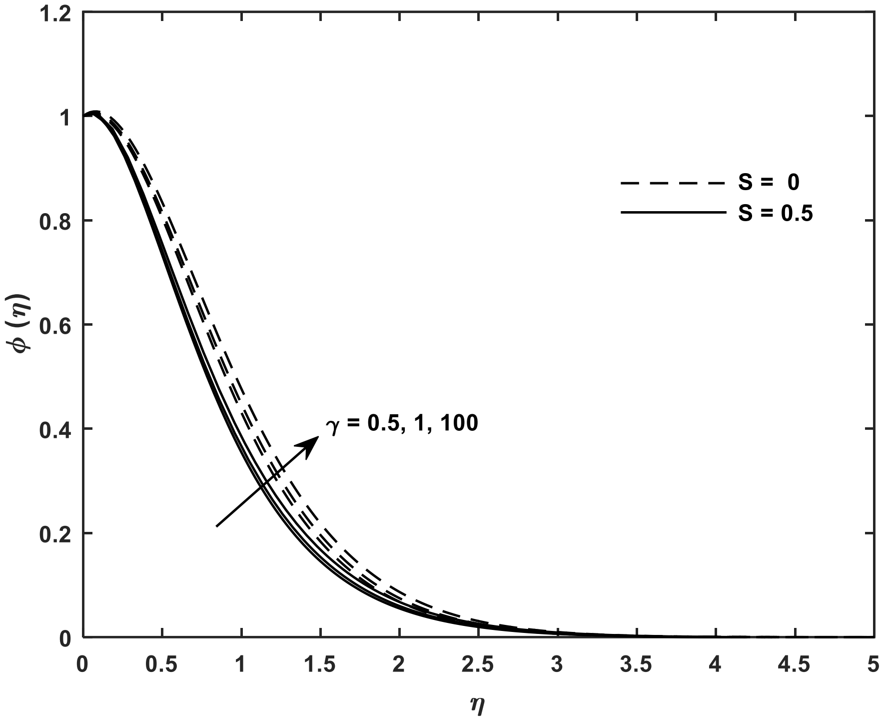

Fig 11: Concentration distributions versus S and γ

Table 2: Computation of $f''(0), -\theta'(0)$ and $-\phi'(0)$ when $Kp = \gamma = 0.5, Nb = Nt = 0.3, n = 2.$

M	β	S	Pr	R	Ec	Sc	Q_e	$-f''(0)$	$-\theta'(0)$	$-\phi'(0)$
0.1	0.1	0	2	0.1	0.1	1	0.1	0.690075	1.593641	0.662945
0.5								0.763479	1.548217	0.663050
1								0.846787	1.490263	0.668581
	0.3							0.695486	1.550537	0.722526
	0.5							0.521781	1.606041	0.767754
		0.5						0.550046	1.959737	0.885626
		1						0.577368	2.259591	0.990695
			3					0.577368	2.578165	0.779118
			5					0.577368	2.971211	0.508111
				0.3				0.577368	3.473128	0.619323
				0.5				0.577368	3.935834	0.712331
					0.3			0.577368	3.639983	0.839830
					0.5			0.577368	3.341396	0.968801
						2		0.577368	3.080330	2.138669

5		0.577368	2.745269	4.207764
	0.5	0.577368	2.511262	4.277873
	1	0.577368	2.215085	4.367104
	-0.5	0.577368	3.091518	4.104659
	-1	0.577368	3.375783	4.020584

Nomenclature

u,v	Velocities along x and y directions respectively (m/s)	Q_e	Exponential space-based heat source/ sink parameter
a	Stretching rate (s^{-1})	T	Temperature $\left({}^0K\right)$
b	Strength of stagnation flow (s^{-1})	C	Concentration
t	Time (s)	U_e	Ambient fluid velocity (m/s)
B_0	Magnetic field strength	T_w	Temperature of the wall $\left({}^0K\right)$
M	Magnetic parameter	T_∞	Ambient temperature $\left({}^0K\right)$
K	Porosity parameter	C_∞	Ambient concentration
n	Exponential index		*Greek Symbols*
$\Pr$	Prandtl number	η	Similarity variable
Nb	Brownian motion parameter	σ	Electrical conductivity $\left(\Omega^{-1}m^{-1}\right)$
Nt	Thermophoresis parameter	ψ	Stream function
Sc	Schmidt number	λ	Positive constant
R	Radiation parameter	γ	Casson parameter
S	Unsteadiness parameter	β	Stretching ratio parameter
D_B	Brownian diffusion coefficient (m^2/s))	α	Thermal diffusivity
D_T	Thermophoresis diffusion coefficient(m^2/s)	τ	Ratio of the nanoparticle heat capacity to the base fluid heat capacity
c_p	Specific heat at constant temperature	$(\rho c)_f$	Heat parameter of base fluid (J/kg K)
Q	heat source/sink parameter	$(\rho c)_p$	Heat parameter of nanoparticle(J/kg K)
k	Thermal conductivity coefficient (m^2/s)	μ_f	Dynamic viscosity of base fluid(kg/m s)
K^*	Permeability of the medium	υ_f	Kinematic viscosity of base fluid(m^2/s)
Q	Heat source/sink coefficient	ρ_f	Density of base fluid (kg/m^3)

Acknowledgements

The authors wish to convey their sincere gratitude to the reviewers for their comments and suggestions to improve the quality of the manuscript.

References

[1] L. J. Crane, Flow past a stretching plate, *Zeitschrift für angewandte Mathematik und Physik ZAMP*, Vol. 21, No. 4, pp. 645-647, 1970.

[2] T. Mahapatra, A. Gupta, Heat transfer in stagnation-point flow towards a stretching sheet, *Heat and Mass transfer,* Vol. 38, No. 6, pp. 517-521, 2002.

[3] J. Misra, A. Sinha, Effect of thermal radiation on MHD flow of blood and heat transfer in a permeable capillary in stretching motion, *Heat and Mass Transfer,* Vol. 49, No. 5, pp. 617-628, 2013.

[4] S. Mukhopadhyay, P. R. De, K. Bhattacharyya, G. Layek, Casson fluid flow over an unsteady stretching surface, *Ain Shams Engineering Journal,* Vol. 4, No. 4, pp. 933-938, 2013.

[5] G. Seth, R. Tripathi, M. Mishra, Hydromagnetic thin film flow of Casson fluid in non-Darcy porous medium with Joule dissipation and Navier's partial slip, *Applied Mathematics and Mechanics,* Vol. 38, No. 11, pp. 1613-1626, 2017.

[6] D. Gopal, N. Kishan, C. Raju, Viscous and Joule's dissipation on Casson fluid over a chemically reacting stretching sheet with inclined magnetic field and multiple slips, *Informatics in medicine Unlocked,* Vol. 9, pp. 154-160, 2017.

[7] P. Sreenivasulu, T. Poornima, N. B. Reddy, Influence of joule heating and non-linear radiation on MHD 3D dissipating flow of casson nanofluid past a non-linear stretching sheet, *Nonlinear Engineering,* Vol. 8, No. 1, pp. 661-672, 2019.

[8] M. Abd El-Aziz, A. A. Afify, MHD Casson fluid flow over a stretching sheet with entropy generation analysis and Hall influence, *Entropy,* Vol. 21, No. 6, pp. 592, 2019.

[9] M. Das, G. Mahanta, S. Shaw, S. Parida, Unsteady MHD chemically reactive double-diffusive Casson fluid past a flat plate in porous medium with heat and mass transfer, *Heat Transfer—Asian Research,* Vol. 48, No. 5, pp. 1761-1777, 2019.

[10] C. K. Kumar, S. Srinivas, A. S. Reddy, MHD pulsating flow of Casson nanofluid in a vertical porous space with thermal radiation and Joule heating, *Journal of Mechanics,* Vol. 36, No. 4, pp. 535-549, 2020.

[11] B. Gireesha, C. Srinivasa, N. Shashikumar, M. Macha, J. Singh, B. Mahanthesh, Entropy generation and heat transport analysis of Casson fluid flow with viscous and Joule heating in an inclined porous microchannel, *Proceedings of the Institution of Mechanical Engineers, Part E: Journal of Process Mechanical Engineering,* Vol. 233, No. 5, pp. 1173-1184, 2019.

[12] B. Kumar, S. Srinivas, Unsteady hydromagnetic flow of Eyring-Powell Nanofluid over an inclined permeable stretching sheet with joule heating and thermal radiation, *Journal of applied and computational mechanics,* Vol. 6, No. 2, pp. 259-270, 2020.

[13] M. A. El-Aziz, A. Afify, Effect of Hall current on MHD slip flow of Casson nanofluid over a stretching sheet with zero nanoparticle mass flux, *Thermophysics and Aeromechanics,* Vol. 26, No. 3, pp. 429-443, 2019.

[14] S. Ibrahim, P. Kumar, G. Lorenzini, E. Lorenzini, Influence of Joule heating and heat source on radiative MHD flow over a stretching porous sheet with power-law heat flux, *Journal of Engineering Thermophysics,* Vol. 28, No. 3, pp. 332-344, 2019.

[15] K. Das, P. R. Duari, P. K. Kundu, Nanofluid flow over an unsteady stretching surface in presence of thermal radiation, *Alexandria engineering journal,* Vol. 53, No. 3, pp. 737-745, 2014.

[16] B. Nagaraja, B. Gireesha, Exponential space-dependent heat generation impact on MHD convective flow of Casson fluid over a curved stretching sheet with chemical reaction, *Journal of Thermal Analysis and Calorimetry,* Vol. 143, No. 6, pp. 4071-4079, 2021.

[17] B. Rout, S. Mishra, Thermal energy transport on MHD nanofluid flow over a stretching surface: a comparative study, *Engineering science and technology, an international journal,* Vol. 21, No. 1, pp. 60-69, 2018.

[18] B. Mahanthesh, G. Lorenzini, F. M. Oudina, I. L. Animasaun, Significance of exponential space-and thermal-dependent heat source effects on nanofluid flow due to radially elongated disk with Coriolis and Lorentz forces, *Journal of Thermal Analysis and Calorimetry,* Vol. 141, No. 1, pp. 37-44, 2020.

[19] S. R. Asemi, A. Farajpour, H. R. Asemi, M. Mohammadi, Influence of initial stress on the vibration of double-piezoelectric-nanoplate systems with various boundary conditions using DQM, *Physica E: Low-dimensional Systems and Nanostructures,* Vol. 63, pp. 169-179, 2014.

[20] S. R. Asemi, A. Farajpour, M. Mohammadi, Nonlinear vibration analysis of piezoelectric nanoelectromechanical resonators based on nonlocal elasticity theory, *Composite Structures,* Vol. 116, pp. 703-712, 2014.

[21] S. R. Asemi, M. Mohammadi, A. Farajpour, A study on the nonlinear stability of orthotropic single-layered graphene sheet based on nonlocal elasticity theory, *Latin American Journal of Solids and Structures,* Vol. 11, No. 9, pp. 1515-1540, 2014.

[22] M. Baghani, M. Mohammadi, A. Farajpour, Dynamic and Stability Analysis of the Rotating Nanobeam in a Nonuniform Magnetic Field Considering the Surface Energy, *International Journal of Applied Mechanics,* Vol. 08, No. 04, pp. 1650048, 2016.

[23] M. Danesh, A. Farajpour, M. Mohammadi, Axial vibration analysis of a tapered nanorod based on nonlocal elasticity theory and differential quadrature method, *Mechanics Research Communications,* Vol. 39, No. 1, pp. 23-27, 2012.

[24] A. Farajpour, M. Danesh, M. Mohammadi, Buckling analysis of variable thickness nanoplates using nonlocal continuum mechanics, *Physica E: Low-dimensional Systems and Nanostructures,* Vol. 44, No. 3, pp. 719-727, 2011.

[25] A. Farajpour, M. H. Yazdi, A. Rastgoo, M. Loghmani, M. Mohammadi, Nonlocal nonlinear plate model for large amplitude vibration of magneto-electro-elastic nanoplates, *Composite Structures,* Vol. 140, pp. 323-336, 2016.

[26] A. Farajpour, M. Mohammadi, A. Shahidi, M. Mahzoon, Axisymmetric buckling of the circular graphene sheets with the nonlocal continuum plate model, *Physica E: Low-dimensional Systems and Nanostructures,* Vol. 43, No. 10, pp. 1820-1825, 2011.

[27] A. Farajpour, A. Rastgoo, M. Mohammadi, Surface effects on the mechanical characteristics of microtubule networks in living cells, *Mechanics Research Communications,* Vol. 57, pp. 18-26, 2014/04/01/, 2014.

[28] A. Farajpour, A. Rastgoo, M. Mohammadi, Vibration, buckling and smart control of microtubules using piezoelectric nanoshells under electric voltage in thermal environment, *Physica B: Condensed Matter,* Vol. 509, pp. 100-114, 2017.

[29] A. Farajpour, A. Shahidi, M. Mohammadi, M. Mahzoon, Buckling of orthotropic micro/nanoscale plates under linearly varying in-plane load via nonlocal continuum mechanics, *Composite Structures,* Vol. 94, No. 5, pp. 1605-1615, 2012.

[30] A. Farajpour, M. Yazdi, A. Rastgoo, M. Mohammadi, A higher-order nonlocal strain gradient plate model for buckling of orthotropic nanoplates in thermal environment, *Acta Mechanica,* Vol. 227, No. 7, pp. 1849-1867, 2016.

[31] M. R. Farajpour, A. Rastgoo, A. Farajpour, M. Mohammadi, Vibration of piezoelectric nanofilm-based electromechanical sensors via higher-order non-local strain gradient theory, *Micro & Nano Letters,* Vol. 11, No. 6, pp. 302-307, 2016.

[32] N. GHAYOUR, A. SEDAGHAT, M. MOHAMMADI, WAVE PROPAGATION APPROACH TO FLUID FILLED SUBMERGED VISCO-ELASTIC FINITE CYLINDRICAL SHELLS, *JOURNAL OF AEROSPACE SCIENCE AND TECHNOLOGY (JAST),* Vol. 8, No. 1, pp. -, 2011.

[33] M. Goodarzi, M. Mohammadi, A. Farajpour, M. Khooran, Investigation of the effect of pre-stressed on vibration frequency of rectangular nanoplate based on a visco-Pasternak foundation, 2014.

[34] H. Mohammadi, M. Ghayour, A. Farajpour, Analysis of free vibration sector plate based on elastic medium by using new version of differential quadrature method, *Journal of Simulation and Analysis of Novel Technologies in Mechanical Engineering,* Vol. 3, No. 2, pp. 47-56, 2010.

[35] H. Moosavi, M. Mohammadi, A. Farajpour, S. H. Shahidi, Vibration analysis of nanorings using nonlocal continuum mechanics and shear deformable ring theory, *Physica E: Low-dimensional Systems and Nanostructures,* Vol. 44, No. 1, pp. 135-140, 2011/10/01/, 2011.

[36] A. G. Arani, S. Maghamikia, M. Mohammadimehr, A. Arefmanesh, Buckling analysis of laminated composite rectangular plates reinforced by SWCNTs using analytical and finite element methods, *Journal of mechanical science and technology,* Vol. 25, No. 3, pp. 809-820, 2011.

[37] M. Mohammadi, M. Goodarzi, M. Ghayour, S. Alivand, Small scale effect on the vibration of orthotropic plates embedded in an elastic medium and under biaxial in-plane pre-load via nonlocal elasticity theory, 2012.

[38] M. Mohammadi, A. Farajpour, M. Goodarzi, R. Heydarshenas, Levy Type Solution for Nonlocal Thermo-Mechanical Vibration of Orthotropic Mono-Layer Graphene Sheet Embedded in an Elastic Medium, *Journal of Solid Mechanics,* Vol. 5, No. 2, pp. 116-132, 2013.

[39] M. Mohammadi, M. Goodarzi, M. Ghayour, A. Farajpour, Influence of in-plane pre-load on the vibration frequency of circular graphene sheet via nonlocal continuum theory, *Composites Part B: Engineering,* Vol. 51, pp. 121-129, 2013.

[40] M. Mohammadi, M. Ghayour, A. Farajpour, Free transverse vibration analysis of circular and annular graphene sheets with various boundary conditions using the nonlocal continuum plate model, *Composites Part B: Engineering,* Vol. 45, No. 1, pp. 32-42, 2013.

[41] M. Mohammadi, A. Farajpour, M. Goodarzi, H. Mohammadi, Temperature Effect on Vibration Analysis of Annular Graphene Sheet Embedded on Visco-Pasternak Foundation *Journal of Solid Mechanics,* Vol. 5, No. 3, pp. 305-323, 2013.

[42] M. Mohammadi, A. Farajpour, M. Goodarzi, H. Shehni nezhad pour, Numerical study of the effect of shear in-plane load on the vibration analysis of graphene sheet embedded in an elastic medium, *Computational Materials Science,* Vol. 82, pp. 510-520, 2014/02/01/, 2014.

[43] M. Mohammadi, A. Farajpour, A. Moradi, M. Ghayour, Shear buckling of orthotropic rectangular graphene sheet embedded in an elastic medium in thermal environment, *Composites Part B: Engineering,* Vol. 56, pp. 629-637, 2014.

[44] M. Mohammadi, A. Farajpour, M. Goodarzi, F. Dinari, Thermo-mechanical vibration analysis of annular and circular graphene sheet embedded in an elastic medium, *Latin American Journal of Solids and Structures,* Vol. 11, pp. 659-682, 2014.

[45] M. Mohammadi, A. Moradi, M. Ghayour, A. Farajpour, Exact solution for thermo-mechanical vibration of orthotropic mono-layer graphene sheet embedded in an elastic medium, *Latin American Journal of Solids and Structures,* Vol. 11, No. 3, pp. 437-458, 2014.

[46] M. Safarabadi, M. Mohammadi, A. Farajpour, M. Goodarzi, Effect of surface energy on the vibration analysis of rotating nanobeam, 2015.

[47] H. Asemi, S. Asemi, A. Farajpour, M. Mohammadi, Nanoscale mass detection based on vibrating piezoelectric ultrathin films under thermo-electro-mechanical loads, *Physica E: Low-dimensional Systems and Nanostructures,* Vol. 68, pp. 112-122, 2015.

[48] M. Goodarzi, M. Mohammadi, M. Khooran, F. Saadi, Thermo-Mechanical Vibration Analysis of FG Circular and Annular Nanoplate Based on the Visco-Pasternak Foundation, *Journal of Solid Mechanics,* Vol. 8, No. 4, pp. 788-805, 2016.

[49] M. Mohammadi, M. Safarabadi, A. Rastgoo, A. Farajpour, Hygro-mechanical vibration analysis of a rotating viscoelastic nanobeam embedded in a visco-Pasternak elastic medium and in a nonlinear thermal environment, *Acta Mechanica,* Vol. 227, No. 8, pp. 2207-2232, 2016.

[50] M. Mohammadi, M. Hosseini, M. Shishesaz, A. Hadi, A. Rastgoo, Primary and secondary resonance analysis of porous functionally graded nanobeam resting on a nonlinear foundation subjected to mechanical and electrical loads, *European Journal of Mechanics - A/Solids,* Vol. 77, pp. 103793, 2019/09/01/, 2019.

[51] M. Mohammadi, A. Rastgoo, Nonlinear vibration analysis of the viscoelastic composite nanoplate with three directionally imperfect porous FG core, *Structural Engineering and Mechanics, An Int'l Journal,* Vol. 69, No. 2, pp. 131-143, 2019.

[52] M. Mohammadi, A. Rastgoo, Primary and secondary resonance analysis of FG/lipid nanoplate with considering porosity distribution based on a nonlinear elastic medium, *Mechanics of Advanced Materials and Structures,* Vol. 27, No. 20, pp. 1709-1730, 2020/10/15, 2020.

[53] M. Mohammadi, A. Farajpour, A. Moradi, M. Hosseini, Vibration analysis of the rotating multilayer piezoelectric Timoshenko nanobeam, *Engineering Analysis with Boundary Elements,* Vol. 145, pp. 117-131, 2022/12/01/, 2022.

[54] P. D. Prasad, S. Saleem, S. Varma, C. Raju, Three dimensional slip flow of a chemically reacting Casson fluid flowing over a porous slender sheet with a non-uniform heat source or sink, *Journal of the Korean Physical Society,* Vol. 74, No. 9, pp. 855-864, 2019.

[55] C. Raju, N. Sandeep, S. Saleem, Effects of induced magnetic field and homogeneous–heterogeneous reactions on stagnation flow of a Casson fluid, *Engineering Science and Technology, an International Journal,* Vol. 19, No. 2, pp. 875-887, 2016.

[56] C. Amanulla, A. Wakif, Z. Boulahia, M. Suryanarayana Reddy, N. Nagendra, Numerical investigations on magnetic field modeling for Carreau non-Newtonian fluid flow past an isothermal sphere, *Journal of the Brazilian Society of Mechanical Sciences and Engineering,* Vol. 40, No. 9, pp. 1-15, 2018.

[57] C. Amanulla, N. Nagendra, M. S. Reddy, Computational analysis of non-Newtonian boundary layer flow of nanofluid past a semi-infinite vertical plate with partial slip, *Nonlinear Engineering,* Vol. 7, No. 1, pp. 29-43, 2018.

[58] C. Amanulla, N. Nagendra, M. S. Reddy, Numerical Simulations on Magnetohydrodynamic Non-Newtonian Nanofluid Flow Over a Semi-Infinite Vertical Surface with Slipeffects, *Journal of Nanofluids,* Vol. 7, No. 4, pp. 718-730, 2018.

[59] C. Amanulla, S. Saleem, A. Wakif, M. AlQarni, MHD Prandtl fluid flow past an isothermal permeable sphere with slip effects, *Case Studies in Thermal Engineering,* Vol. 14, pp. 100447, 2019.

[60] S. M. Upadhya, C. Raju, S. Saleem, Nonlinear unsteady convection on micro and nanofluids with Cattaneo-Christov heat flux, *Results in Physics,* Vol. 9, pp. 779-786, 2018.

[61] M. J. Babu, N. Sandeep, S. Saleem, Free convective MHD Cattaneo-Christov flow over three different geometries with thermophoresis and Brownian motion, *Alexandria Engineering Journal,* Vol. 56, No. 4, pp. 659-669, 2017.

[62] N. Nagendra, C. Amanulla, M. S. Reddy, V. R. Prasad, Hydromagnetic flow of heat and mass transfer in a nano Williamson fluid past a vertical plate with thermal and momentum slip effects: numerical study, *Nonlinear Engineering,* Vol. 8, No. 1, pp. 127-144, 2019.

[63] N. Nallagundla, C. Amanulla, M. S. Reddy, Mathematical analysis of non-Newtonian nanofluid transport phenomena past a truncated cone with Newtonian heating, *Journal of Naval Architecture and Marine Engineering,* Vol. 15, No. 1, pp. 17-35, 2018.

[64] R. Kumar, V. Gupta, I. A. Abbas, Plane deformation due to thermal source in fractional order thermoelastic media, *Journal of computational and theoretical nanoscience*, Vol. 10, No. 10, pp. 2520-2525, 2013.

[65] A. D. Hobiny, I. A. Abbas, Fractional order thermoelastic wave assessment in a two-dimension medium with voids, *Geomechanics and Engineering,* Vol. 21, No. 1, pp. 85-93, 2020.

[66] S. Horrigue, I. A. Abbas, Fractional-Order Thermoelastic Wave Assessment in a Two-Dimensional Fiber-Reinforced Anisotropic Material, *Mathematics*, Vol. 8, No. 9, pp. 1609, 2020.

[67] M. Marin, A. Hobiny, I. Abbas, The effects of fractional time derivatives in porothermoelastic materials using finite element method, *Mathematics*, Vol. 9, No. 14, pp. 1606, 2021.

[68] T. Saeed, I. A. Abbas, The Effect of Fractional Time Derivative on Two-Dimension Porous Materials Due to Pulse Heat Flux, *Mathematics,* Vol. 9, No. 3, pp. 207, 2021.

[69] A. Abdalla, I. Abbas, H. Sapoor, The effects of fractional derivatives of bio-heat model in living tissues using analytical-numerical method, *Information Sciences Letters,* Vol. 11, No. 1, pp. 6, 2022.

[70] T. Hayat, T. Muhammad, S. Shehzad, G. Chen, I. A. Abbas, Interaction of magnetic field in flow of Maxwell nanofluid with convective effect, *Journal of Magnetism and Magnetic Materials,* Vol. 389, pp. 48-55, 2015.

[71] M. S. Ram, N. Ashok, S. Salawu, M. Shamshuddin, Significance of cross diffusion and uneven heat source/sink on the variable reactive 2D Casson flowing fluid through an infinite plate with heat and Ohmic dissipation, *International Journal of Modelling and Simulation*, pp. 1-15, 2022.

[72] M. Shamshuddin, M. R. Eid, nth order reactive nanoliquid through convective elongated sheet under mixed convection flow with joule heating effects, *Journal of Thermal Analysis and Calorimetry,* Vol. 147, No. 5, pp. 3853-3867, 2022.

[73] M. Shamshuddin, W. Ibrahim, Finite element numerical technique for magneto-micropolar nanofluid flow filled with chemically reactive Casson fluid between parallel plates subjected to rotatory system with electrical and Hall currents, *International Journal of Modelling and Simulation*, pp. 1-20, 2022.

[74] M. Shamshuddin, F. Mebarek-Oudina, S. Salawu, A. Shafiq, Thermophoretic Movement Transport of Reactive Casson Nanofluid on Riga Plate Surface with Nonlinear Thermal Radiation and Uneven Heat Sink/Source, *Journal of Nanofluids,* Vol. 11, No. 6, pp. 833-844, 2022.

[75] F. Mabood, M. Shamshuddin, S. Mishra, Characteristics of thermophoresis and Brownian motion on radiative reactive micropolar fluid flow towards continuously moving flat plate: HAM solution, *Mathematics and Computers in Simulation,* Vol. 191, pp. 187-202, 2022.

[76] G. R. Rajput, M. Shamshuddin, S. O. Salawu, Thermosolutal convective non-Newtonian radiative Casson fluid transport over a vertical plate propagated by Arrhenius kinetics with heat source/sink, *Heat Transfer,* Vol. 50, No. 3, pp. 2829-2848, 2021.

[77] M. Senapati, K. Swain, S. K. Parida, Numerical analysis of three-dimensional MHD flow of Casson nanofluid past an exponentially stretching sheet, *Karbala Int. J. Mod. Sci,* Vol. 6, No. 1, pp. 93-102, 2020.

[78] K. Swain, S. Parida, G. Dash, MHD heat and mass transfer on stretching sheet with variable fluid properties in porous medium, *AMSE J Model B,* Vol. 86, pp. 706-726, 2017.

[79] S. K. Das, S. U. Choi, W. Yu, T. Pradeep, 2007, *Nanofluids: science and technology*, John Wiley & Sons,

Numerical Solution and MATLAB code

The dimensionless coupled nonlinear ordinary differential equations (6) - (9) are solved numerically by Runge-Kutta fourth order method with shooting technique using MATLAB code with step length $\Delta\eta = 0.01$ and the error tolerance 10^{-5}. In this method, the equations are reduced to a set of first order differential equations:

$$y_1' = y_2,$$

$$y_2' = y_3,$$

$$y_3' = -\left(1+\gamma^{-1}\right)^{-1}\left[y_1y_3 - y_2^2 - \left(M + K_p\right)\left(y_2 - \beta\right) + \beta^2 - S\left(\frac{1}{2}\eta y_3 + y_2 - \beta\right)\right],$$

$$y_4' = y_5,$$

$$y_5' = \Pr\left(1+\frac{4}{3}R\right)^{-1}\begin{bmatrix} S\left(\frac{1}{2}\eta y_7 + 2y_4\right) - y_1y_5 + 2y_2y_4 - Nby_5y_7 - Nty_5^2 \\ -MEcy_2^2 - Ec\left(1+\gamma^{-1}\right)y_3^2 - Q_e\exp\left(-n\eta\right) \end{bmatrix},$$

$$y_6' = y_7,$$

$$y_7' = Sc\left[S\left(\frac{1}{2}\eta y_7 + 2y_6\right) - fy_7 + 2y_2y_6 - \frac{Nt}{ScNb}y_5'\right],$$

with the initial conditions

$$y_1(0) = 0, y_2(0) = 1, y_4(0) = 1, y_6(0) = 1.$$

Now, the initial value problem is solved by appropriately guessing the missing initial values i.e. $y_3(0), y_5(0),$ and $y_6(0)$ using shooting technique for various sets of parameters. There is an inbuilt self-corrective procedure in the MATLAB coding (bvp4c code) to correct the unknown guess values.